Conformational Heterogeneity in RNA Polymerase Observed by Single-Pair FRET Microscopy

Oana Coban,* Don C. Lamb,*† Evgeny Zaychikov,‡ Hermann Heumann,‡ and G. Ulrich Nienhaus*†
*Department of Biophysics, University of Ulm, Ulm, Germany; †Department of Physics, University of Illinois at Urbana-Champaign, Urbana, Illinois; and ‡Max-Planck Institute for Biochemistry, Martinsried, Germany

ABSTRACT Kinetic, structural, and single-molecule transcription measurements suggest that RNA polymerase can adopt many different conformations during elongation. We have measured the geometry of the DNA and RNA in ternary elongation complexes using single-pair fluorescence resonance energy transfer. Six different synthetic transcription elongation complexes were constructed from DNA containing an artificial transcription bubble, an RNA primer, and core RNA polymerase from *Escherichia coli*. Two different RNA primers were used, an 8-mer and a 5′-extended 11-mer. Fluorescent dye labels were attached at one of three positions on the DNA and at the RNA primer 5′-end. Structurally, the upstream DNA runs perpendicular to the proposed RNA exit channel. Upon nucleoside-triphosphate addition, DNA/RNA hybrid separation occurs readily in the 11-mer complexes but not in the 8-mer complexes. Clear evidence was obtained that RNA polymerase exists in multiple conformations among which it fluctuates.

INTRODUCTION

RNA polymerase (RNAP) from *Escherichia coli* (*E. coli*) is the enzyme responsible for the synthesis of all RNA in this organism. During transcription, RNA is assembled according to the sequence of nucleotides on the DNA template strand at specific regions recognized by the RNAP. In this process, RNAP catalyzes the formation of a phosphodiester bridge between the 3′-end of the nascent RNA and the α-phosphate of an incoming nucleoside triphosphate (NTP). RNAP moves along the DNA strand by using the energy liberated from the hydrolysis of the NTP. In addition, RNAP is responsible for recognition of the transcription start site on the DNA (promoter) as well as transcription termination. Therefore, the whole process of RNA synthesis is divisible into three distinct processes: initiation, elongation, and termination.

Bulk kinetic measurements (1,2), structure determinations (3–7), and single molecule studies of elongation (8–10) all suggest that RNAP exists in many different conformational states. In this work, we have used fluorescence resonance energy transfer (FRET) to study structural heterogeneity and dynamics of RNAP. FRET is a sensitive optical method that requires the presence of two fluorescent dyes in close proximity. They are referred to as donor (D) and acceptor (A) fluorophores. Upon excitation of the donor, energy can be transferred nonradiatively to the acceptor, with an efficiency that depends on their spatial separation. The FRET effect covers distances of up to ~100 Å and is sensitive to changes in the donor-acceptor (D-A) separation on the 1−2 Å scale. Therefore, the technique is well suited for studying conformational changes within biomolecules as well as protein-protein and protein-nucleic acid interactions. A number of excellent reviews on FRET can be found in the literature (11–15). FRET has also been applied to structural studies of RNAP (16–21).

The FRET technique can also be exploited in single-molecule fluorescence experiments. Single-pair FRET (spFRET) was first demonstrated by Ha et al. (22) and since then has been applied to single- and double-stranded DNA, RNA, and proteins (23–29). Single molecule studies have clear advantages over ensemble experiments. They allow the observation and investigation of different subpopulations within an ensemble. Moreover, kinetic information can be obtained from processive enzymes such as RNAP. Additionally, complexes that are inactive, not properly labeled, or show other types of anomalous behavior can be excluded from the final analysis.

As a first step in analyzing the transcription dynamics of RNAP, we have used spFRET to investigate conformational heterogeneity and flexibility of the transcription elongation complex (TEC) comprising a DNA duplex, an RNA primer, and RNAP, in which the DNA and RNA were labeled with a FRET dye pair. By this approach, we avoided the difficulties associated with specific labeling of the RNAP near the active site and were still able to investigate the structure of the DNA and RNA strands within the TEC. The FRET efficiencies of the individual complexes were measured using far-field confocal fluorescence microscopy with dual-color detection. From these data, we analyzed the structure of the complexes and the changes accompanying elongation. Moreover, the distributions in D-A separations were analyzed for static and

Submitted November 30, 2005, and accepted for publication March 8, 2006.

Address reprint requests to Prof. Dr. G. Ulrich Nienhaus, Tel.: 49-731-502-3050; E-mail: uli@uiuc.edu; or Don C. Lamb, Tel.: 49-89-2180 -77564; E-mail: don.lamb@cup.uni-muenchen.de.

Oana Coban's present address is Steacie Institute for Molecular Sciences, National Research Council Canada, Ottawa, ON K1A 0R6, Canada.

Don C. Lamb's present address is Physical Chemistry, Dept. of Chemistry and Biochemistry, Ludwig-Maximilians-Universität München, Butenandtstr. 11 Haus E, 81377 Munich, Germany.

© 2006 by the Biophysical Society

0006-3495/06/06/4605/13 $2.00

doi: 10.1529/biophysj.105.078840

dynamic heterogeneity, including structural fluctuations accompanying elongation. Upon elongation, the ability of the DNA/RNA hybrid to dissociate was investigated using complexes prepared with an 8-mer RNA and an 11-mer RNA, providing insight into the conformation transition in RNAP complex at RNA lengths of 9–10 nucleotides.

MATERIALS AND METHODS

Protein purification

Core RNAP was prepared from *E. coli* B cells according to Burgess and Jendrisak (30) with final purification on BioRex70 resin (BioRad Laboratories, Hercules, CA), providing 100% removal of the σ-subunit and >95% pure core enzyme, as verified using SDS-gel analysis. More than 90% of the molecules were active in complex formation with artificial bubble DNA that was stable against heparin.

Double-labeled DNA

A 171-basepair DNA that contained two internally attached fluorophores separated by 16 bases was prepared by enzymatic ligation of synthetic DNA fragments. The DNA sequence was taken at the A1 promoter site of bacteriophage T7 from position −91 to +80. According to convention, +1 is defined as the position where transcription begins; the adjacent position upstream is denoted as position −1. The fluorescent labels were introduced at positions –4 and +13 on the template strand via C6 amino linkers attached to the C5 position of a modified thymine nucleotide and reacted with *n*-hydroxysuccinimidyl ester derivatives of Cy3 (Amersham Biosciences, Piscataway, NJ) or Cy5 (Amersham Biosciences). The DNA fragments were ligated separately into upper and lower strands using short fragments of the opposite strand as a staple. Full-length strands were purified by HPLC, annealed, and separated from the nonligated DNA by HPLC.

Artificial bubble template

The following DNA and RNA constructs were used for the artificial bubble complexes:

```
 -18      -10        +1        +10        +20
  |        |         |         |          |
              TAGCACTCC
5´ACTTACAGCC          GACACGGCGAATAGCCATCCC-3' NT Strand
3´TGAATGTCGG          CTGTGCCGCTTATCGGTAGGG-5´  T Strand
            TAGCACTCC
            AUCGUGAG    8mer RNA primer (R8)
          AUUAUCGUGAG   11mer RNA primer (R11)
```

The upper and lower strands of the DNA 40-mer are complementary with the exception of an internal nine-base region. The noncomplementary region does not basepair, causing an artificial bubble in the DNA similar to the transcription bubble formed by RNAP during RNA synthesis. The DNA strands were purchased (IBA GmbH, Göttingen, Germany and MWG Biotech, Ebersberg, Germany) or synthesized at the University of Ulm and purified to >95% homogeneity by ion-exchange HPLC on monoQ resin (Amersham Bioscience) using a MiLiChrom chromatograph (EcoNova, Novosibirsk, Russia). The DNA strands were modified with an amino linker in one of following locations: 1), 5′-end of the nontemplate strand (position –18), the C5 carbon of a thymine-modified base at 2), position −2 on the nontemplate strand; and 3), at position –12 of the template strand. The strands were fluorescently labeled by reacting them with Cy3 NHS (Amersham Biosciences). Biotin was attached to the nonlabeled strand at the upstream end. Duplex DNA was obtained by mixing template and nontemplate strands at a 1:1 molar ratio, heating to 90°C, followed by slow cooling to room temperature. The final duplex was purified using ion-exchange HPLC.

Two different RNA primers were used, an 8-mer (5′-AUCGUGAG) that was complementary to the template strand from position −8 to −1 and an 11-mer (5′-AUUAUCGUGAG) that was also complementary from position −8 to −1 and extended by three bases at the 5′-end that were noncomplementary to either strand of the DNA. The primers were supplied by IBA GmbH, reacted with Alexa Fluor 647 carboxylic acid, succinimidyl ester (Molecular Probes Europe, Leiden, Netherlands) and purified using HPLC.

Artificial bubble complex formation

DNA template (100 pmol) was incubated with 150 pmol of core RNAP in 100 μl BBh20 buffer (20 mM HEPES at pH 7.5, 6 mM $MgCl_2$, 20 mM NaCl, and 5 mM mercaptoethanol) for 5 min at 37°C. RNA primer (200 pmol) was added and incubated for another 5 min. Then, the mixture was applied to a 1-ml heparin-superose column (Amersham Biosciences), which was washed with 3 ml TDEG buffer (50 mM Tris-HCl at pH8, 1 mM EDTA, 5 mM mercaptoethanol, 5% glycerol w/v) containing 50 mM NaCl. The TECs were eluted from the column with 2 ml of TDEG buffer containing 400 mM NaCl. Free core enzyme was eluted from the column with TDEG containing 1 M NaCl. The TEC fraction was concentrated and desalted by four repetitive centrifugation-dilution cycles on Nanosep-100 units (Pall Life Sciences, Ann Arbor, MI) and concentrated to a final volume of 50 μl. The complex could be stored at +4°C for several days without any significant loss in the transcriptional activity.

Effect of labels on the TEC

The yield of ternary complex formation was unaffected by labels on either the DNA and or on the RNA primer. The stability of nonlabeled TEC and TEC formed with labeled DNA and RNA against heparin was tested by incubation of TEC with heparin and analyzing their integrity using nondenaturing gel electrophoresis. No significant difference in the stability of the labeled and unlabeled complexes was observed. The elongation competence of the TECs was tested by incubating nucleotides to the TEC for a preset time and analyzing the length of the nascent RNA strand using denaturing gel electrophoresis. The fluorescent labels used in this work had no significant impact on the fraction of transcriptionally competent TECs and the kinetics of elongation. In contrast, fluorescent labels placed on the template strand at position −1 or +1 greatly diminished the yield of TEC formation and hinders transcription.

Preparation of samples for FRET measurements

A flow cell was constructed from a quartz slide with two holes and a coverslip, held together with double-sided adhesive tape. Before assembly, a channel was cut into the tape connecting the two holes in the quartz slide. The TEC was attached to the surface of the quartz slide using a biotin-streptavidin-biotin linkage. The surface of the sample holder was first saturated with biotinylated

BSA (Sigma-Aldrich, St. Louis, MO) by incubation with a 1-mg/ml solution (20 mM potassium phosphate buffer, pH 7.4) for 10 min. The sample holder was rinsed with buffer and then flushed with a streptavidin solution (300 μg/ml in 20 mM potassium phosphate buffer) (Molecular Probes Europe). After another 10 min, it was rinsed once again and the sample (at ~20 pM) was added to the holder. The sample was diluted from a stock solution of 100–500 nM immediately before application to the surface. All measurements were performed with degassed buffer in the presence of oxygen scavengers following the recipe of Kim et al. (31). The buffer for the elongation experiments was 10 mM HEPES, 6 mM $MgCl_2$, 50 mM NaCl, 1 mM mercaptoethanol, with a pH of 7.5.

Experimental setup for single molecule FRET measurements

Single molecule experiments were performed on an epi-fluorescence microscope (Axiovert 135 TV, Zeiss, Jena, Germany) with two-channel confocal detection. The sample was excited with an argon-krypton ion laser (modified Model 164, Spectra-Physics, Mountain View, CA) operated at 514 nm. The laser light was delivered to the microscope via a single-mode fiber (HPUC, OZ Optics, Carp, Canada), collimated and reflected via a dichroic mirror (532/633 DCXR, AHF, Tübingen, Germany) into the objective (C-Apochromat, 63 × W Korr, NA = 1.2, Zeiss), and focused to a diffraction-limited spot. The total laser power at the sample was less than 5 μW, corresponding to a power density of 25 $\mu W/\mu m^2$. The fluorescence signal was collected via the same objective, passed through the dichroic mirror, focused on a pinhole (80 μm) for the confocal geometry, and directed to two avalanche photodiodes (SPCM-AQR, EG&G Optoelectronics Canada, Vaudreuil, Canada) via a dichroic beamsplitter (650 DCXR, AHF) for detection. The output of the avalanche photodiodes was recorded using a homebuilt photon-counting card and software. Images were created by scanning the sample in two dimensions through the observation volume using a piezo stage (P-731.20, Physik Instrumente, Karlsruhe, Germany) with feedback control.

Data collection and analysis

The FRET efficiency of the individual molecules was calculated using the formula

$$E = \frac{I_A}{\alpha I_D + I_A}, \quad (1)$$

where α is a correction factor for the detection efficiency of the donor channel relative to the acceptor channel, and I_D and I_A are the fluorescence intensities of the donor and acceptor channels, respectively. The intensities were calculated by integrating the detected photons in a 4 × 4 pixel area (560 × 560 nm^2) at the fluorescence spot in both channels. The average backgrounds of the green and red channels were subtracted from the respective signals. During the analysis, the images of the individual molecules were visually inspected for abnormalities. Molecules that bleached during the experiment, overlapped spatially with other molecules, or were sitting in regions with an inhomogeneous or high fluorescent background were removed from the analysis. The α-factor was determined from spFRET bleaching experiments for each dye pair by comparing the intensity of both channels before bleaching of the acceptor to that of the donor after beaching of the acceptor. For our system, α was equal to 1.0. Crosstalk of the donor fluorescence into the acceptor channel was removed by multiplying the intensity of the donor channel with the experimentally determined crosstalk ratio of 5% and subtracting the result from the intensity of the acceptor channel before calculation of the FRET efficiency.

The D-A separation, R, was calculated using

$$R = R_0 \left(\frac{\alpha I_D}{I_A} \right)^{\frac{1}{6}}, \quad (2)$$

where R_0 is the Förster radius (i.e., the distance at which the energy transfer efficiency is 50%). The Förster radius is dependent on the relative orientation of the donor and acceptor dipole, the quantum yield of the donor, and the index of refraction of the surrounding media. Using an orientation factor of 2/3 and the measured quantum yield of Cy3 attached internally to double-stranded DNA, we calculated an R_0 of 53 Å for the Cy3-Cy5 FRET pair, using an index of refraction of 1.33, in agreement with Ishii et al. (28). R_0 = 51 Å was obtained for the Cy3-Alexa647 FRET pair. In the latter case we used an index of refraction of 1.4 (32) to account for the fact that the space between the donor and acceptor molecule is filled mostly with protein rather than buffer.

Multiple regions of the sample were scanned either three or six times during an experiment. Fresh buffer was flushed through the sample holder between successive scans to avoid buildup of gluconic acid generated from the reaction of glucose with oxygen in the presence of glucose oxidase. Any shift of the sample during the experiment was corrected by cross-correlating each subsequent scan with the previous image. The shift, if any, was determined from the peak of the cross-correlation function. The analysis routine automatically selected individual molecules requiring a minimum number of 50 detected photons from the molecule in each scan.

Influence of the surface on the TEC

The elongation competence of TEC bound to the surface was tested by measuring the length of the RNA strand produced after NTP addition. Complexes were tethered to the surface at higher concentrations than those used for single molecule studies and excess complexes were rinsed away. After addition of NTPs, the complexes were denatured on the surface and the retrieved RNA analyzed using denaturing gel electrophoresis. Over 95% of the complexes were found to be transcription competent and there was no discernable difference between measurements of surface complexes and the same complexes measured in solution. In addition, changes in D-A separation upon addition of NTPs were clearly visible for the R11 complexes (see Results and Discussion) using spFRET directly on the surface, suggesting that the functionality of the RNAP was not influenced by the surface. As an additional test of the influence of the surface on the TEC, we also compared biotinylated polyethylene-glycol and biotinylated-BSA surfaces (33). For these measurements, TECs were formed using holoenzyme RNAP, DNA containing a natural promoter site and an 11-mer RNA transcript. The DNA and RNA were labeled similarly to the artificial bubble complex T–12 R8. With both surface preparations, wide distributions containing both high (>70%) and intermediate (between 40% and 70%) FRET efficiencies were observed. Although small differences in the relative populations of the high and intermediate components showed some influence of the surface on the protein, the similar distributions obtained with two chemically different surfaces suggest that our results are not markedly affected by TEC-surface interactions. This view is supported by a number of single-molecule studies of biomolecules on functionalized surfaces from our laboratory (31,34–37).

RESULTS AND DISCUSSION

A feasibility study using double-labeled DNA

FRET is sensitive to donor-acceptor (D-A) separations of 20−100 Å and changes in D-A separation of 1−2 Å, making it an excellent tool for investigating structural heterogeneity in biomolecules. However, the fluorescent markers are often attached via long, flexible linkers that create some uncertainty in the structural interpretation of the D-A separation. In addition, the FRET efficiency also depends on other determinants, including the relative orientations of the donor and acceptor transition dipoles, the donor quantum yield, and

the dielectric environment of the fluorophores. From ensemble measurements, a single FRET efficiency can be obtained, in which the heterogeneity in the ensemble due to various linker conformations or dipolar orientations are averaged out. By using spFRET, we can not only determine the average FRET efficiency, but also measure the shape and width of the FRET efficiency distribution, which provides information on the conformational heterogeneity of biomolecules. However, extreme caution is required when interpreting the origin of any observed distribution.

To explore the possibility of using spFRET for measurements of conformational heterogeneity, we performed control experiments on double-stranded (ds) DNA molecules. In contrast to earlier spFRET measurements on DNA (22,29, 38,39), both donor and acceptor molecules were attached internally, more than 60 bases away from the ends of the DNA, thus avoiding the complication of partial DNA melting at the ends. The D-A separation was 16 bases, corresponding to ~55 Å. The persistence length of dsDNA is ~500 Å (40). Consequently, on the length scale of 55 Å, dsDNA can be treated as a rigid rod, allowing us to test the effects of linker flexibility and DNA-dye interactions on the width of the FRET efficiency distribution.

The flexibility of the donor and acceptor molecules was assessed by measuring the polarization anisotropy on an ensemble. The donor and acceptor showed rather high bulk anisotropies, r_0, of 0.34 and 0.32, respectively, indicating that the orientations of the transition dipole moments of both dyes are rather fixed on the timescale of the fluorescence lifetime.

For single molecule measurements, the DNA fragment was attached to the surface by means of a biotin-streptavidin linkage, with a biotin molecule bound to the 5′-end of the nonfluorescently labeled DNA-strand. A schematic representation of the experiment is shown in Fig. 1 *a*. The donor and acceptor fluorescence intensities of individual DNA strands were detected in separate channels as the sample was raster-scanned across the confocal detection volume (shown as *green*, *yellow*, and *red dots* in Fig. 1 *b* depending on the relative intensity of the two channels). The FRET efficiency and the D-A separations of 188 single double-stranded DNA molecules were calculated as described in Materials and

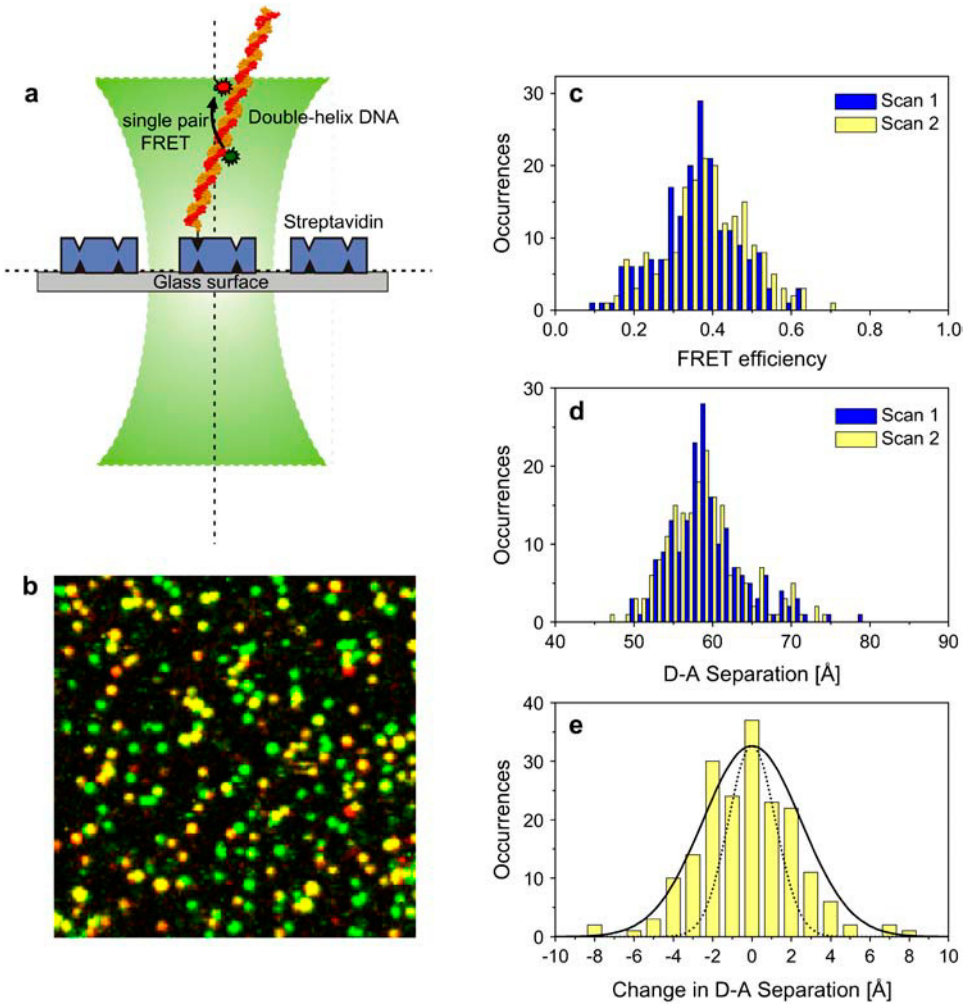

FIGURE 1 SpFRET study of surface-tethered DNA molecules. (*a*) Pictorial representation of the experimental geometry. (*b*) Fluorescence image of individual, double-labeled DNA molecules, with low, medium, and high energy transfer efficiencies shown in green, yellow, and red, respectively. (*c*) Histograms of FRET efficiencies measured in two consecutive scans. (*d*) Distributions of donor-acceptor distances for the double-labeled DNA from two consecutive scans. The inter-dye distances were calculated using $R_0 = 53$ Å for the (Cy3,Cy5) dye pair. (*e*) Histogram of the changes in donor-acceptor separation between consecutive scans. The lines represent a Gaussian fit of the actual distribution (*solid line*) and a simulated Gaussian with width as expected for a shot-noise broadened distribution (*dotted line*).

Methods. A particular advantage of single molecule over bulk experiments is the possibility of selecting subpopulations of the sample to incorporate in the analysis. Consequently, we have only included those molecules in the analysis that had both a donor fluorophore and a fluorescently active acceptor molecule. The histogram of measured FRET efficiencies and D-A separations are shown in Fig. 1, *c* and *d*, respectively.

We characterize the distributions by calculating averages and standard deviations. For the distribution of FRET efficiencies in Fig. 1 *c*, the average is 0.36 ± 0.01, and the standard deviation is 0.10 ± 0.01. In Fig. 1 *d* and in all following figures, we present the spFRET results as distributions in the apparent D-A separation rather than in FRET efficiency because the distribution in FRET efficiency originates from variations in the distance between donor and acceptor. Hence, the shape of the distribution is most accurately represented with respect to apparent D-A separation. However, we note here that different orientations of the donor and acceptor would also contribute to the distribution of apparent distances.

The distribution in D-A separations in Fig. 1 *d* spans a range of 50 to 75 Å, with an average of 58.7 ± 0.4 Å (statistical accuracy) and a standard deviation of 4.9 Å, respectively. Using a molecular model of DNA, the distance between the attachment points is 57.1 Å. A three-dimensional cylindrical model of DNA (39,41) yields a value ranging from 55.6 to 57.6 Å, depending on the distance from the DNA axis chosen for the donor and acceptor. Hence, our peak of the measured distribution of D-A separations is in quantitative agreement with the expected value for a linear piece of B DNA.

In addition to the average D-A separation, the width of the distribution contains information about sample heterogeneity, which may originate from different conformations of the linker attaching the dye to the DNA, different orientations of the donor and acceptor transition dipoles, and/or different DNA conformations. The distribution in D-A separations can be either static (heterogeneous) or dynamic (homogeneous). In the static or heterogeneous case, each molecule is fixed in a specific conformation with a well-defined D-A separation over the time interval probed in the experiment. The distribution then arises because the different molecules in the ensemble assume a different conformation. In the dynamic or homogeneous case, each molecule fluctuates among all possible structures. If the fluctuations are fast compared to the timescale of the measurement, only the average value will be observed and the width of the distribution is limited by the precision of the measurement. If the dynamics are on the timescale of the measurement, the FRET distribution will be broad because the various molecules are in different structures during the measurement. A second measurement at a time longer than the time required for the molecules to fluctuate between different structures will show the same overall distribution, but the individual molecules will have D-A separations very different from those in the first measurement. Hence, by comparing the FRET distribution measured on the same ensemble of individual complexes at different times, we can distinguish between homogenous and heterogeneous broadening of the distribution on the timescale of the experiment.

We measured the FRET efficiency of the identical molecules a second time after a delay of 10 min. The distributions of FRET efficiencies and D-A separations, shown in yellow in Fig. 1, *c* and *d*, respectively, are very similar to the first measurement shown in blue. In addition, Fig. 1 *e* shows the histogram of the change in D-A separation for the individual molecules between the first and the second scan. The standard deviation of the distribution of the change in D-A separation is 2.5 Å, which is significantly less than the width of the distribution of D-A separations (4.9 Å). This difference indicates that the distribution of D-A separations has a static component on the 10-min timescale. The width of the distribution of the change in D-A separation is significantly larger than expected from photon counting statistics. The error in apparent D-A separation for each molecule can be determined from the photon counts measured in each channel. More than 96% of the molecules have an uncertainty from photon statistics of <1.2 Å (standard deviation). A Gaussian distribution with standard deviation of 1.2 Å (and one with 2.5 Å for comparison) is shown in Fig. 1 *e*. Evidently, the width of the distribution is not solely governed by photon counting statistics but contains an additional component. This additional component may be due to conformational fluctuations of the dyes and linkers on the DNA, but could also be due to the triplet transitions of the acceptor or nonidentical detection volumes. Here we use this experiment merely as a control to show that widths of FRET distributions >2.5 Å indicate significant sample heterogeneity. A quantitative interpretation of FRET distributions of double-labeled DNA is not within the scope of this work.

Artificial bubble complexes

The analysis of three-dimensional structures of ternary complexes of DNA, RNA and RNAP has been the goal of many investigations (5,6,18,21,42,43). However, general agreement on an unambiguous model has not yet been achieved. Furthermore, information on the functional dynamics is desirable but not easily available from x-ray crystallography. A model structure of the TEC from *Thermus aquaticus* (Fig. 2 *a*, courtesy of Seth Darst), assembled from x-ray data of the protein and complemented by results from chemical cross-linking and mutational analysis for portions of the DNA and RNA positions, gives a suggestion of how DNA (template strand in *orange* and nontemplate strand in *brown*) and RNA (in *blue*) may be threaded through the RNAP in the TEC.

In our spFRET experiments, we have investigated the structure and dynamics of TECs using a total of six different synthetic transcription complexes (three DNA constructs $\times$ two RNAs). The complex contained DNA with an internal

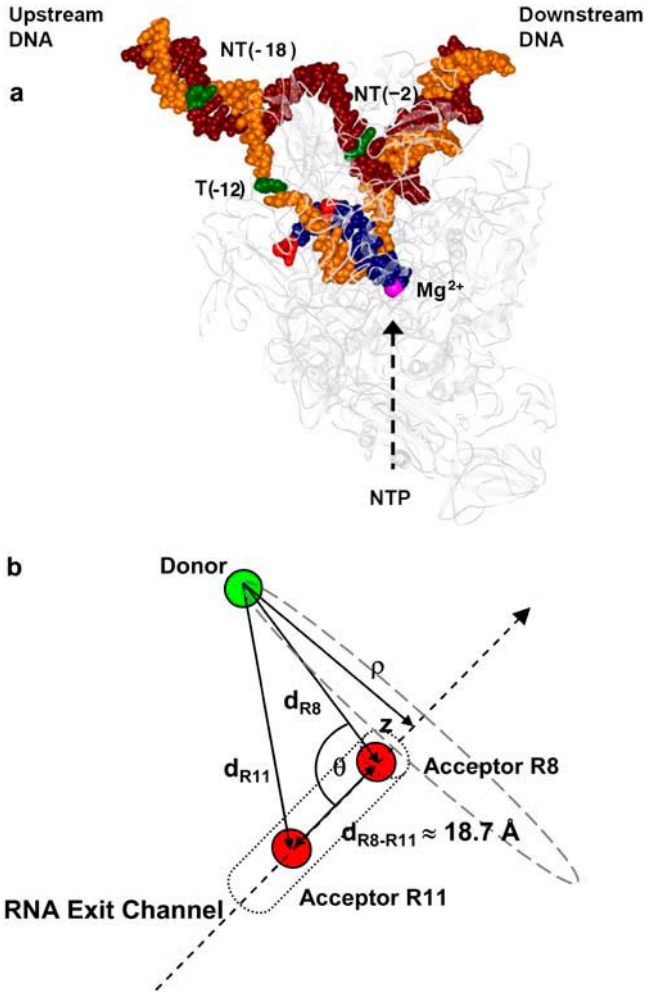

FIGURE 2 (*a*) Structural model of the *E. coli* transcription elongation complex (courtesy of S. Darst, Rockefeller University, NY). The DNA template strand is shown in orange, the nontemplate strand in brown and the RNA in dark blue. The nucleotides to which the donor and acceptor labels were attached are shown in green and red, respectively. The protein moiety is depicted in shading. The Mg^{2+} ion in the active site of the protein is represented by a magenta sphere. The dashed arrow indicates the path of incoming nucleotide substrates to the active site. (*b*) Graphic visualization of the location of the donor to within a circle about the RNA exit channel, calculated from the distances between the donor and the acceptor of the R8 (d_{R8}) and R11 (d_{R11}) complexes and the separation of the R8 and R11 RNA ($d_{R8\text{-}R11}$).

artificial bubble of nine unmatched bases and an RNA primer, as described in Materials and Methods. Two different RNA primers were used, an 8-mer (R8), which was complementary to the first eight bases of the artificial bubble region of the template strand, and an 11-mer (R11) containing the sequence of the 8-mer primer plus a noncomplementary upstream (or 5′-end) extension of AUU. Von Hippel and co-workers (44–46) have previously shown that artificial bubble complexes are transcriptionally competent. The artificial bubble TECs have similar stability and functional properties as the TECs formed using natural, fully double-stranded (mismatch-free) DNA containing a promoter site. However, artificial bubble TECs do not elongate the nascent RNA efficiently to a termination site or to the end of the DNA strand.

The RNA primers were labeled with a FRET acceptor (Alexa 647, Molecular Probes) on the 5′-end. The DNA was labeled with a donor (Cy3, Amersham Bioscience) on the nontemplate strand at position −18 (NT−18) or −2 (NT−2), or on the template strand at position −12 (T−12). The nucleotides to which the linker of the donor was attached to the DNA are shown in green and the locations of the 5′-ends of the RNA to which the acceptor molecule was attached are shown in red. As discussed in Materials and Methods, the stability and elongation properties of the fluorescently labeled complexes were not influenced by the labeling.

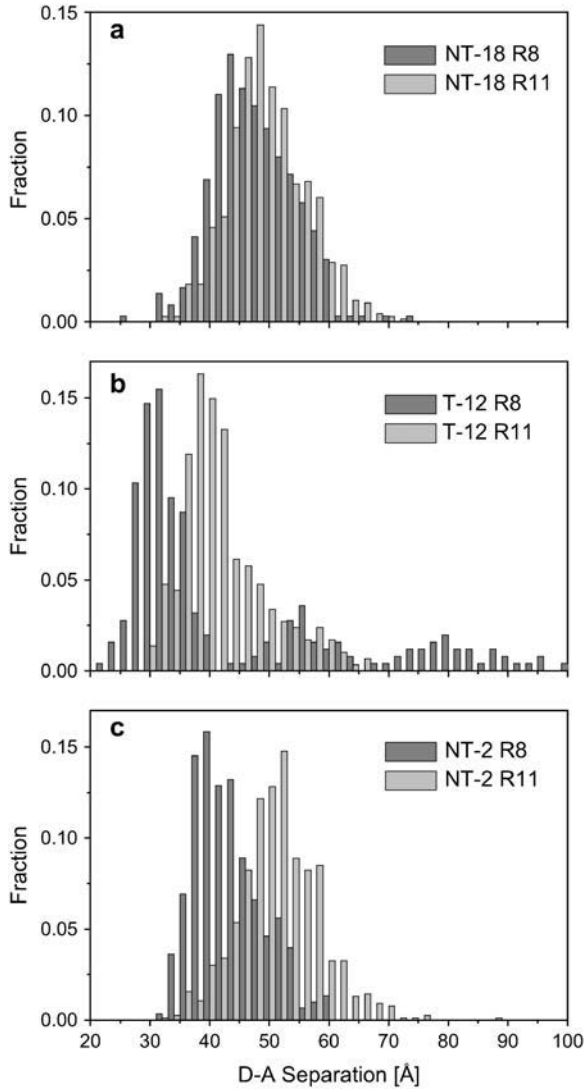

FIGURE 3 Distributions of donor-acceptor distances on TECs from spFRET measurements. The acceptor molecule was always attached at the 5′-end of the RNA. The donor was located on the DNA strand in one of the following positions: (*a*) NT−18, (*b*) T−12, (*c*) NT−2. Complexes were assembled using R8 (*dark shading*) and R11 (*light shading*) primers.

The FRET efficiencies of individual TECs were measured for all six constructs described above. The measurements were repeated a total of six times on the same molecules. Three scans were taken before incubating the sample for 2 min with 50 μM ATP, GTP, and CTP, and three scans were taken afterwards. Histograms of D-A separations from the first three scans are shown in Fig. 3. As with the double-labeled DNA, we have only included complexes in the analysis that contained both a donor and an acceptor molecule.

Averages and standard deviations of the D-A distance distributions of the various complexes are given in Table 1. The standard deviations of the distributions are significantly larger than the 2.5 Å resolution of our apparatus as determined from the measurements on the double-labeled DNA, indicating that the D-A separations of the TEC complexes are distributed. From the measurements, we have also calculated the change in D-A separation that each complex underwent between scans (Table 1). The reproducibility of the measurements using independent sample preparations was better than 5 Å. Anisotropies were measured in ensemble measurements for both donor and acceptor molecules of all complexes; they were found to reside in the range of 0.30−0.39.

For the NT–18 and NT–2 complexes, the distributions in D-A separations have a single peak and are symmetric. Two conformations can be distinguished for the T−12 R11 complex. In contrast, three different structural conformations are observed for the T−12 R8 complex from the distribution of D-A separations in Fig. 3 *b*, with peaks occurring around 30, 55, and 80 Å. However, as the peak at 80 Å was not observed in the other five complexes, it may not represent functional TECs and will thus not be discussed further.

Structural conformation of the TEC

The FRET data enable us to extract information on the three-dimensional structure of the TEC. Assuming that the 5′-end of the 11-mer primer mimics a strand of extended single-stranded RNA within the RNA exit channel, we can determine the location of the donor to within a circle about the axis of the RNA exit channel (Fig. 2 *b*). Assuming that the model reasonably approximates the structure of the 5′-end of the RNA, the distance between the labeling positions of the R8 and R11 complexes is 18.7 Å. The radius of the circle (ρ) and the distance between the 5′-end of the R8 RNA and the plane of the circle (z) were calculated for the three different DNA labels and are included in Table 2. For the NT−18 and T−12 complexes, the angle between the R11 and R8 acceptors and the R8 acceptor and the donors, θ, is ~90°. The donors reside in a plane perpendicular to the RNA exit channel that is within ±4 Å of the R8 acceptor. Because R8 is fully complementary to the template strand, we can infer that the upstream DNA runs perpendicular to the proposed RNA exit channel. In contrast, the plane containing the donor in the NT−2 complex is ~13.1 Å above the R8 acceptor.

The accuracy of the measurements in D-A separation can be checked by comparing the measured values with the calculated distances between the attachment points of the linkers of the structural model (Table 2). For the NT–18 complex, the agreement is good. However, there are significant differences for the other two complexes (T−12 and NT−2). In fact, the D-A separation for the T−12 R8 complex of 34.8 Å (or 31.1 Å for the first peak alone) is impossible if the DNA and RNA are still hybridized at position −8 and the dyes are localized around their attachment points. The T−12 position of the template stand is separated from the 5′-end of the RNA by four bases and should thus have a separation of ~20 Å instead of 34.8 Å. This discrepancy between the distanced measured using FRET and the model of the T−12 complex can be explained by noting a key difference between the NT−18 complex on the one hand and the T−12 and NT−2 complexes on the other hand: The donor label is external to the RNAP in the NT−18 complex and internal to the protein in the latter two complexes. In the DNA channel, conformational space is severely restricted. For the internally labeled DNA, the linker consists of 18 carbon-carbon and carbon-nitrogen bonds

TABLE 1 Averages and standard deviations (SD) of distributions of D-A separations and their temporal changes for the six measured complexes determined both before and after addition of NTPs

			Distribution of D-A separations before addition of NTPs			Distribution of D-A separations after addition of NTPs		
Complexes	RNA primer	Measured number of molecules	Average [Å]	SD [Å]	SD of the change in D-A separation [Å]	Average [Å]	SD [Å]	SD of the change in D-A separation [Å]
DNA	—	188	58.7 ± 0.3	4.9 ± 0.2	2.5 ± 0.1			
NT (−18)	R8	121	46.5 ± 0.4	6.7 ± 0.3	5.3 ± 0.2	48.1 ± 0.4	6.7 ± 0.3	4.2 ± 0.2
	R11	255	48.7 ± 0.2	6.6 ± 0.2	5.5 ± 0.2	53.1 ± 0.2	6.1 ± 0.2	5.0 ± 0.2
T (−12)	R8	72*	40.8 ± 1.2	17.5 ± 0.8	4.7 ± 0.3	42.6 ± 1.2	17.0 ± 0.8	5.5 ± 0.3
		62†	34.8 ± 0.7	9.1 ± 0.5	3.7 ± 0.2	36.7 ± 0.6	8.5 ± 0.4	5.2 ± 0.3
		52‡	31.1 ± 0.3	3.5 ± 0.2	3.8 ± 0.3	33.6 ± 0.4	4.8 ± 0.3	5.5 ± 0.4
	R11	94	41.0 ± 0.4	7.1 ± 0.3	4.9 ± 0.3	47.1 ± 0.4	6.9 ± 0.3	5.6 ± 0.3
NT (−2)	R8	101	42.3 ± 0.3	5.7 ± 0.2	5.5 ± 0.3	43.3 ± 0.3	5.9 ± 0.2	5.4 ± 0.3
	R11	189	51.3 ± 0.3	6.4 ± 0.2	5.5 ± 0.2	52.4 ± 0.2	5.4 ± 0.2	4.9 ± 0.2

*Parameters for the entire distribution.
†Parameters for the first two peaks (all molecules with D-A separation <65 Å).
‡Parameters for the first peak (all molecules with D-A separation <43 Å).

TABLE 2 Comparison of the measured D-A separations to the structural model, with parameters *z*, ρ, and θ as shown in Fig. 2 *b*

Complexes	RNA primer	Average D-A distance before elongation [Å]	Model D-A separation [Å]	Triangulation (z) Å	Triangulation (ρ) Å	Triangulation (θ) degrees
NT (−18)	R8	$46.5^{52.3}_{44.1}$	47.5	$-3.8^{-1.2}_{-4.4}$	$46.3^{52.3}_{43.9}$	$85.3^{88.7}_{84.2}$
	R11	$48.7^{55.2}_{46.2}$	51.4			
T (−12)	R8	$34.8^{39.3}_{32.9}$	19.8	$3.2^{5.9}_{2.1}$	$34.7^{38.8}_{32.8}$	$95.2^{98.7}_{93.6}$
	R11	$41.0^{46.0}_{38.9}$	24.2			
NT (−2)	R8	$42.3^{48.1}_{40.0}$	24.8	$13.1^{20.2}_{10.5}$	$40.2^{43.7}_{38.6}$	$108.1^{114.8}_{105.2}$
	R11	$51.3^{58.5}_{48.5}$	43.8			

The minimum and maximum ranges in the D-A separation arising from uncertainties in κ^2 are shown as subscripts and superscripts, respectively.

between the thymine base and the aromatic moiety of the Cy3 dye. As we demonstrated with our control experiments on double-labeled DNA in Fig. 1, the average D-A separation, as determined from the FRET efficiency, faithfully reproduces the distance between the attachment points on the DNA, even though the dyes were attached to the DNA by fairly long, flexible linkers. If the linkers are able to fluctuate symmetrically at their point of attachment, they are expected to increase the width of the distribution but not alter the average distance. However, if the dyes are attached to locations internal to the TEC where there are steric hindrances and energetic costs to burying the charged chromophore, this assumption may no longer be valid. The long, flexible linkers can allow the dyes to stick to charged moieties on the protein surface even though the attachment point is within the TEC. For consistency, we have averaged the two populations with the shortest D-A separation for the T−12 R8 complex (Fig. 3 *b*). The conclusions derived in this work are unaffected if only the conformation with the shortest D-A distance is considered.

There is still a discrepancy between the structural model and the measured results for the NT−2 complexes that cannot be explained by the linker alone. In the model, the −2 position of the nontemplate strand is directly above the RNA exit channel. This can be seen from the fact that, in the model, the change in distance between the donor at position NT−2 and the acceptor on the 5′-end of the R8 and R11 RNA strands (19 Å, Table 2) is essentially the same as the distance between the 5′-end of the R8 and R11 strands (18.7 Å). For our measurement, the donor is 40 Å away from the axis of the RNA exit channel. As was seen with the T−12 complexes, the internal environment of the protein displaces the fluorophore by a significant distance from the attachment point. A fully extended linker can only cover ~20 Å, suggesting that the structural arrangement of the single-stranded portion of the nontemplate strand in the model does not describe the actual structure of the TEC.

The precision with which distances can be determined by FRET depends on the accuracy to which the Förster distance, R_0, is known. Uncertainties in R_0 arise from the determination of the orientation factor, the index of refraction, and from changes in the quantum yield of the donor. The R_0 values used in this study assume an orientation factor of 2/3, which is only valid for flexible or randomly oriented dipoles. Anisotropy studies of the TEC show bulk anisotropies in the range 0.30–0.39 for both donor and acceptor. These large values imply that the rotational freedom of the dyes is severely restricted, which may cast doubt on the assumption of 2/3 for the orientation factor. However, the high FRET efficiencies of the T−12 R8 and R11 complexes and intermediate FRET efficiencies of the other complexes suggest that the orientation factor is not at either extreme. We have estimated the uncertainty in κ^2 (using Eq. 36 in (11)) assuming that the steady-state anisotropy comes from rotation of the fluorophores, which is much faster than rotation of the protein. From these estimates, the extreme values of κ^2 for our complexes are between 0.47 and 1.47. The absolute uncertainties in D-A separation due to κ^2 are given in Table 2. The accuracy of FRET measurements is also affected by the index of refraction. In our system, the acceptor, and for most TEC constructs also the donors are buried inside the protein, where the refractive index, n, is different than that of the solvent. As discussed by Parkhurst et al. (47), the effective index of refraction governing the coupling between the donor and acceptor transition dipoles is a nontrivial issue because the dye environment is heterogeneous. Typically, for a dye within a protein, n may be estimated as ~1.4, a value between that of buffer (1.33) and protein (1.5) (32). As n enters the Förster distance expression to the power 2/3, the maximum error on the accuracy of D-A separation is 4% when using the refractive index of 1.4. The Förster distance also depends on the lifetime of the donor (although the rate of energy transfer only depends on the intrinsic lifetime of the fluorophore). Fluorescent labels in biological complexes are frequently observed to undergo a change in quantum yield due to interactions of the dye with the proteins or nucleic acids. This effect also needs to be considered carefully to avoid additional errors in the determination of the D-A separation.

Conformational heterogeneity of the TEC

For a more detailed look at conformational heterogeneity of RNAP complexes, we have compared the width of the full distribution in D-A separation with that of the change in D-A separation between consecutive scans, in analogy to what

was done for the control measurements on double-labeled DNA. The same molecules were scanned three times at intervals of ~10 min. The results are included in Table 1. For the T−12 R8 complex, the width of the distribution was determined with and without inclusion of the second and third peaks. For the NT−18 R8 and R11, T−12 R8 and R11, and NT−2 R11 complexes, the standard deviation of the change in D-A separation between scans is less than the width of the entire distribution. The distribution of the changes in the D-A distance, however, is too broad to be attributed to experimental uncertainty (as determined from the control measurements on double-labeled DNA), indicating that the distribution in D-A separations contains both homogenous and heterogeneous components. With the NT−2 R8 complex and to a lesser extent the NT−2 R11 complex (upon addition of NTPs), the change in D-A separation has a similar width to the distribution of the D-A separations. With this complex, the distribution is homogenous, suggesting that the structure of the nontemplate strand is not strongly influenced by the distinct conformations of the TEC.

The homogenous and heterogeneous broadening of the distribution of the D-A separations can be demonstrated graphically by comparing the width of the full distribution with that of a selected subpopulation, as depicted in Fig. 4. Fig. 4, *a* (R8) and *c* (R11), show the histogram of D-A separations (*dark shading*) for the first scan of the NT−18 complexes. Molecules with an initial D-A separation between 40 and 45 Å are marked in light shading. The histogram of D-A separations of the subsequent two scans are shown in Fig. 4, *b* (R8) and *d* (R11), in dark shading for all molecules and in light shading for the subpopulation selected from scan 1. The molecules with an initial D-A separation between 40−45 Å remain on the lower side of the distribution on the timescale of our measurement (10 min between scans). In a purely homogenously broadened distribution of D-A separations, a selected subpopulation would recover the full width of the entire distribution if the time interval between successive scans is longer than the timescale of fluctuations from one conformation to another. Subpopulations of a heterogeneously broadened distribution would retain the narrow width upon subsequent scans. From the heterogeneous broadening of the distribution of D-A separations, we infer that there are different overall structures of the TEC, which are stable on the 10-min timescale.

The homogenous broadening of the distribution in D-A separations demonstrates that the TEC is flexible. The width of the homogeneous broadening is in the range of 5.0−5.5 Å, with the exception of the T−12 R8 complex, which shows the largest amount of heterogeneous broadening and appears to be tightly constrained. All labeling positions have a similar flexibility, even though the NT−2 complexes were labeled on the single-stranded portion of the nontemplate strand. Hence, from the homogenous broadening, the TEC exists in a subset of different structural conformations among which it fluctuates incessantly under physiological conditions.

DNA/RNA hybrid separation

Fig. 5 shows the results of spFRET experiments in the form of D-A separation histograms of the six TEC constructs before (*dark shading*) and after addition of NTPs (*light shading*). The histograms of the R8 complexes (Fig. 5, *a–c*) are similar before and after NTP addition, with only small changes in the D-A separation, regardless of the position of the fluorescent label. In contrast, the distributions clearly shift upon NTP addition to the R11 complexes (Fig. 5, *d–f*). Bulk solution experiments also revealed larger changes in FRET efficiency upon the addition of NTPs for the R11

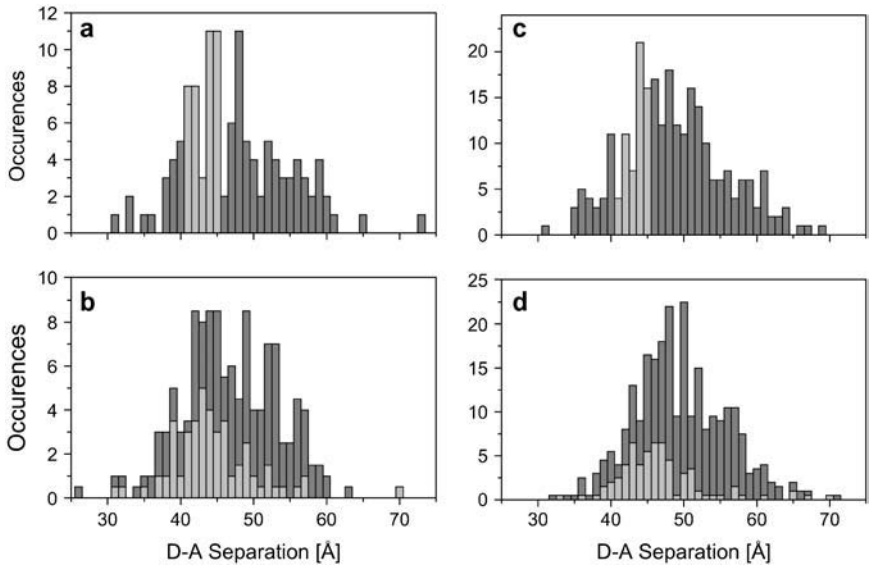

FIGURE 4 Conformational heterogeneity of the NT−18 TECs. The distributions of donor-acceptor distances are plotted for the complexes assembled with R8 (*a*,*b*) and R11 (*c*,*d*) primers. Histograms are shown for: (*a*) Full distribution (*dark shading*) and the fraction of molecules with donor-acceptor separations between 40 and 45 Å (*light shading*) measured in the first scan. (*b*) Full distribution (*dark shading*) and the fraction of molecules with initial donor-acceptor separations between 40 and 45 Å (*light shading*) measured in the second and third scans. (*c*) Full distribution (*dark shading*) and the fraction of molecules with donor-acceptor separations between 40 and 45 Å (*light shading*), measured in the first scan. (*d*) Full distribution (*dark shading*) and the fraction of molecules with donor-acceptor separations between 40 and 45 Å (*light shading*) measured in the second and third scans.

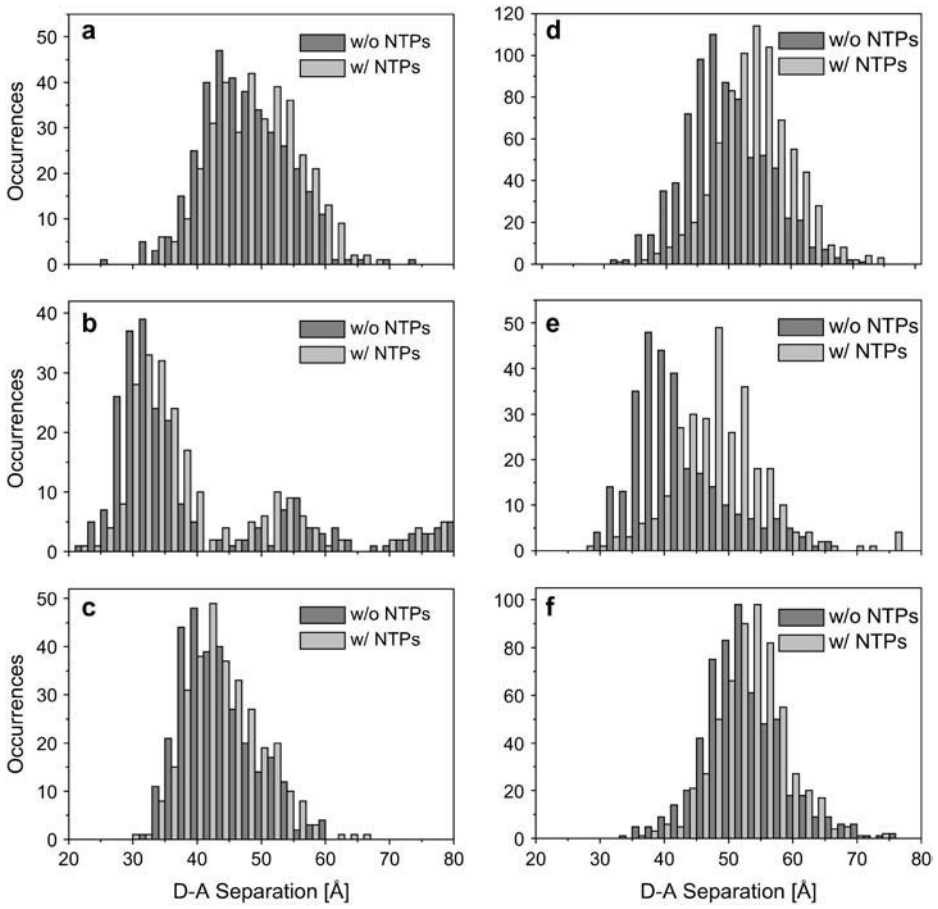

FIGURE 5 Donor-acceptor distances of the different complexes before (*dark shading*) and after (*light shading*) addition of NTPs. Histograms are shown for complexes (*a*) NT−18 R8, (*b*) T−12 R8, (*c*) NT−2 R8, (*d*) NT−18 R11, (*e*) T−12 R11, and (*f*) NT−2 R11.

complexes with respect to the R8. We verified the functionality of our artificial bubble complexes by elongating samples in solution and analyzing the RNA product using gel electrophoresis. Both the R8 and R11 RNA could be extended by three bases (to position +3) with ATP and GTP substrates and to position +5/+6 with the addition of ATP, GTP, and CTP nucleotides. Additionally, we verified that the TECs tethered to the surface were functional. Hence, only the R11 complexes show a clear change in D-A separation upon NTP addition although both R8 and R11 complexes undergo elongation.

A structural transition is observed in both bacterial and eukaryotic RNAPs when the transcript has reached a length of 10 nucleotides (48–50). The nascent RNA must separate from the DNA/RNA hybrid and be threaded into the exit channel of the RNAP. The observation that R8 complexes are transcriptionally active and still do not show a change in D-A separation implies that the 5′-end of the RNA does not separate from the complementary DNA strand upon NTP addition. The difference between our complexes and native complexes is the complementary DNA strand competing to rebind to the template DNA strand. Hence, there is no incentive for the RNA to dissociate from the DNA-RNA hybrid. Von Hippel and co-workers also reported that proper RNA displacement was not always observed for artificial bubble complexes (45,46). However, they achieved proper displacement by adding a 1000-fold excess of RNA primer. The excess primer competes for the unpaired DNA bases of the template strand, helping the nascent RNA strand to dissociate from the DNA and exit through the RNA channel.

In contrast to the R8 complexes, R11 complexes, with an RNA primer extended upstream by three noncomplementary bases, showed facile separation of DNA and RNA upon elongation. The marked changes in the D-A separation of the complexes upon addition of NTPs in Fig. 5, *d–f*, suggests that the RNA displaces normally with the 11-mer RNA primer. The RNA has already been threaded into the exit channel, and the complementary DNA is not necessary to continue dissociation of the DNA/RNA hybrid. We also performed experiments using a five-basepair artificial bubble and 8-mer RNA primer (data not shown). Here too, significant changes were observed in D-A separation upon addition of NTPs, both in bulk assays and in single molecule experiments, suggesting that the complementary DNA plays a role in the initial separation of the DNA/RNA hybrid. These results are consistent with measurements performed by Wilson and coworkers using a 12-basepair artificial bubble (51). There, the displacement of the RNA-DNA hybrid was more efficient with a 20-mer RNA primer extended upstream by eight nucleotides than with the 12-mer RNA primer. The extended

primer is presumably located in the RNA exit channel, and after DNA/RNA separation has begun, proper dislocation of the RNA proceeds without difficulties.

Conformational heterogeneity of TECs upon elongation

We also investigated the conformational heterogeneity of the RNAP TECs upon elongation. Fig. 6 shows histograms of D-A separations of the NT−18 R11. The distribution of D-A separations before elongation is shown in Fig. 4 *c*. After elongation with ATP, GTP, and CTP, three more scans were taken at intervals of ~10 min. The distribution from scan 1 after elongation is shown in dark shading in Fig. 6 *a*, the average of scans 2 and 3 in Fig. 6 *b*, and the average of all three scans in Fig. 6 *c*. Highlighted in light shading in Fig. 6, *a* and *b*, are those molecules that showed D-A separations of 45–50 Å in the first scan after NTP addition. In Fig. 6 *b*, the width of the D-A distribution of the highlighted molecules is significantly narrower (standard deviation 4.9 Å) than the width of the entire distribution (standard deviation 6.1 Å). The standard deviations of the corresponding changes in D-A separation are 4.9 and 5.5 Å for the highlighted molecules and the full distribution, respectively. Both widths are less than the 6.1 Å of the entire distribution in D-A separations, indicating that conformational heterogeneity is still present in molecules that have been elongated with NTPs. A comparison of the width of the full distribution to the standard deviation of the change in D-A separation given in Table 1 shows that conformational heterogeneity persists in all elongated complexes (although to a lesser extent in NT−2) on a timescale longer than the experiment.

The highlighted molecules in Fig. 6 *c* are those that had an initial D-A separation of 40–45 Å before addition of NTPs. The width of the distribution of highlighted molecules is similar to the width of the full distribution. This is true for both NT−18 R11 and T−12 R11 complexes, which show a considerable shift in the D-A separation upon addition of NTPs. From this observation, we conclude that the total extent of conformational heterogeneity, as measured here with spFRET, develops fully upon elongation.

To monitor the dynamics of elongation using a FRET pair on the DNA and RNA requires separation of the nascent RNA from the DNA template strand. As we have shown above, this can be achieved by extending the RNA primer upstream. In our experiments, the fraction of complexes that elongated beyond the artificial bubble to the end of the template DNA strand was <2%, which is close to the 4% observed by von Hippel (46). We did not detect any difference in the fraction of complexes that could transcribe through the artificial bubble for the R8 and R11 constructs. For spFRET studies of transcription over many steps, a TEC with a natural promoter site on double-stranded DNA would be useful in conjunction with the labeling scheme on the DNA and RNA employed here.

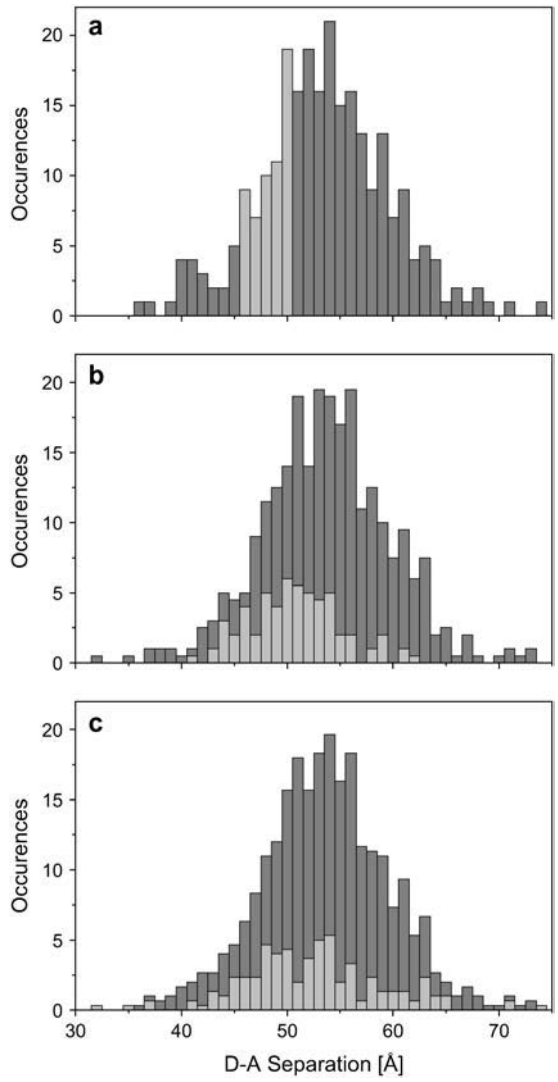

FIGURE 6 Conformational heterogeneity of elongated NT−18 R11 TECs (*a*,*b*) and interconversion among conformations during elongation (*c*). (*a*) Full distribution (*dark shading*) and the fraction of molecules with donor-acceptor separations between 45 and 50 Å (*light shading*) measured in the first scan after the addition of NTPs. (*b*) Full distribution (*dark shading*) and the fraction of molecules marked in light shading in panel *a* (in *light shading* again), measured in the second and third scans after addition of NTPs. (*c*) Full distribution (*dark shading*) overlapped with the fraction of molecules with donor-acceptor distances between 40 and 45 Å before elongation (marked in *light shading* in Fig. 4 *c*), measured in all three consecutive scans after addition of NTPs.

It is generally accepted that the elongation complex of RNAP exists in many different conformational states (1). Flexibility of RNAP has been inferred from several structural studies. Comparison of x-ray structures of yeast RNAP II from different crystal forms suggest mobility in different regions of the protein (3). X-ray crystallography measurements of the holoenzyme of *Thermus aquaticus* RNAP alone and bound to fork-junction DNA show structural variability of the clamp domain and the β-flap (5,6). Van Heel and

co-workers have compared the structures of core and holoenzyme from *E. coli* using cryo-electron microscopy (7) and have identified large conformational rearrangements, particularly in the β'-subunit. To superimpose the two RNAP molecules from *Thermus aquaticus* and *E. coli*, which have a high amount of sequence homology, a conformational change of nearly 25 Å is required at the opening of the DNA/RNA channel (4). This suggests significant conformational freedom precisely in the region of the TEC where our fluorescent markers are located. Using spFRET, we were able to measure distributions in TEC structural conformations and to observe the flexibility of the complexes as they fluctuate between these conformations.

The observed conformational heterogeneity may arise from different conformations of the RNAP that compete kinetically at the identical template position, as was discussed in detail by Greive and von Hippel (52). The majority of the molecules would be in the elongation-active state, but a minority may be in the pretranslocation state, paused state, or arrested state. The conformations of the paused and arrested states can be studied by using single-molecule FRET with DNA templates having sequences known to enhance arrest or backtracking.

CONCLUSIONS

In this study, we have developed a model complex for investigating the structure and function of the RNAP TEC using single-molecule techniques. By analyzing the experimental data one TEC at a time, we could select properly labeled complexes that contained both fluorescently active donors and acceptors. Hence, no correction was necessary for donor-only or acceptor-only complexes. The widths of the distributions could be directly assessed and the static and dynamic components of the heterogeneity determined. For the studies presented here, the distributions were static on the timescale of 10 min in the absence of NTPs. The heterogeneous broadening of the NT−2 complexes was less than observed for the other complexes, suggesting that the structure of the nontemplate DNA is not strongly influenced by the different conformations of the TEC. By comparing the differences in D-A separation for the various complexes, we verified that the RNA channel through which the nascent RNA exits the enzyme is approximately perpendicular to the plane of the template strand. Using spFRET, we could readily observe separation of the DNA/RNA hybrid, which occurred rarely in the R8 complexes but much more frequently in the R11 complexes. This suggests that the complementary DNA strand plays an important role in initiating separation of the DNA/RNA hybrid. For investigating the dynamics of elongation, the artificial bubble complexes appear less well suited. Still, the labeling scheme used here could be incorporated in TECs with DNA containing a natural promoter site and provide a means of measuring dynamic changes in D-A separation. Single-molecule studies with these fluorescent native RNAP TECs will be a powerful approach for detailed investigations of the mechanism of elongation and pausing.

We thank Michael Hinz and Cornelia Egger (University of Ulm) for synthesis of the DNA strands, Seth Darst for supplying the TEC structural model, and Barbara K. Müller and Stefan Paternoster for performing some final control experiments.

We gratefully acknowledge financial support from the Volkswagen Foundation and Sonderforschungsbereich grant No. 569. H.H. also acknowledges support from the European Union under the DLAB contract No. HPRI-CT-2001-50035 and contract No. RII3-CT-2003-505925.

REFERENCES

1. Erie, D. A. 2002. The many conformational states of RNA polymerase elongation complexes and their roles in the regulation of transcription. *Biochim. Biophys. Acta.* 1577:224–239.
2. Foster, J. E., S. F. Holmes, and D. A. Erie. 2001. Allosteric binding of nucleoside triphosphates to RNA polymerase regulates transcription elongation. *Cell.* 106:243–252.
3. Cramer, P., D. A. Bushnell, and R. D. Kornberg. 2001. Structural basis of transcription: RNA polymerase II at 2.8 Ångstrom resolution. *Science.* 292:1863–1876.
4. Darst, S. A., N. Opalka, P. Chacon, A. Polyakov, C. Richter, G. Y. Zhang, and W. Wriggers. 2002. Conformational flexibility of bacterial RNA polymerase. *Proc. Natl. Acad. Sci. USA.* 99:4296–4301.
5. Murakami, K. S., S. Masuda, E. A. Campbell, O. Muzzin, and S. A. Darst. 2002. Structural basis of transcription initiation: an RNA polymerase holoenzyme-DNA complex. *Science.* 296:1285–1290.
6. Murakami, K. S., S. Masuda, and S. A. Darst. 2002. Structural basis of transcription initiation: RNA polymerase holoenzyme at 4 Ångstrom resolution. *Science.* 296:1280–1284.
7. Finn, R. D., E. V. Orlova, B. Gowen, M. Buck, and M. van Heel. 2000. *Escherichia coli* RNA polymerase core and holoenzyme structures. *EMBO J.* 19:6833–6844.
8. Adelman, K., A. La Porta, T. J. Santangelo, J. T. Lis, J. W. Roberts, and M. D. Wang. 2002. Single molecule analysis of RNA polymerase elongation reveals uniform kinetic behavior. *Proc. Natl. Acad. Sci. USA.* 99:13538–13543.
9. Davenport, R. J., G. J. L. Wuite, R. Landick, and C. Bustamante. 2000. Single-molecule study of transcriptional pausing and arrest by *E. coli* RNA polymerase. *Science.* 287:2497–2500.
10. Tolic-Nørrelykke, S. F., A. M. Engh, R. Landick, and J. Gelles. 2004. Diversity in the rates of transcript elongation by single RNA polymerase molecules. *J. Biol. Chem.* 279:3292–3299.
11. Clegg, R. 1996. Fluorescence Resonance Energy Transfer. *In* Fluorescence Imaging Spectroscopy and Microscopy. X. F. Wang and B. Herman, editors. John Wiley & Sons, New York. 170–252.
12. Selvin, P. R. 2000. The renaissance of fluorescence resonance energy transfer. *Nat. Struct. Biol.* 7:730–734.
13. Jares-Erijman, E. A., and T. M. Jovin. 2003. FRET imaging. *Nat. Biotechnol.* 21:1387–1395.
14. Selvin, P. R. 1995. Fluorescence resonance energy transfer. *Methods Enzymol.* 245:300–334.
15. Wu, P., and L. Brand. 1994. Resonance energy transfer: methods and applications. *Anal. Biochem.* 218:1–13.
16. Heyduk, T., and A. Niedziela-Majka. 2001. Fluorescence resonance energy transfer analysis of *Escherichia coli* RNA polymerase and polymerase-DNA complexes. *Biopolymers.* 61:201–213.
17. Heyduk, T. 2002. Measuring protein conformational changes by FRET/LRET. *Curr. Opin. Biotechnol.* 13:292–296.

18. Naryshkin, N., A. Revyakin, Y. G. Kim, V. Mekler, and R. H. Ebright. 2000. Structural organization of the RNA polymerase-promoter open complex. *Cell.* 101:601–611.

19. Mukhopadhyay, J., A. N. Kapanidis, V. Mekler, E. Kortkhonjia, Y. W. Ebright, and R. H. Ebright. 2001. Translocation of $\sigma(70)$ with RNA polymerase during transcription: fluorescence resonance energy transfer assay for movement relative to DNA. *Cell.* 106:453–463.

20. Mukhopadhyay, J., V. Mekler, E. Kortkhonjia, A. N. Kapanidis, Y. W. Ebright, and R. H. Ebright. 2003. Fluorescence resonance energy transfer (FRET) in analysis of transcription-complex structure and function. *Methods Enzymol.* 371:144–159.

21. Mekler, V., E. Kortkhonjia, J. Mukhopadhyay, J. Knight, A. Revyakin, A. N. Kapanidis, W. Niu, Y. W. Ebright, R. Levy, and R. H. Ebright. 2002. Structural organization of bacterial RNA polymerase holoenzyme and the RNA polymerase-promoter open complex. *Cell.* 108:599–614.

22. Ha, T., T. Enderle, D. F. Ogletree, D. S. Chemla, P. R. Selvin, and S. Weiss. 1996. Probing the interaction between two single molecules: fluorescence resonance energy transfer between a single donor and a single acceptor. *Proc. Natl. Acad. Sci. USA.* 93:6264–6268.

23. Zhuang, X., L. E. Bartley, H. P. Babcock, R. Russell, T. Ha, D. Herschlag, and S. Chu. 2000. A single-molecule study of RNA catalysis and folding. *Science.* 288:2048–2051.

24. Talaga, D. S., W. L. Lau, H. Roder, J. Tang, Y. Jia, W. F. DeGrado, and R. M. Hochstrasser. 2000. Dynamics and folding of single two-stranded coiled-coil peptides studied by fluorescent energy transfer confocal microscopy. *Proc. Natl. Acad. Sci. USA.* 97:13021–13026.

25. Schuler, B., E. A. Lipman, and W. A. Eaton. 2002. Probing the free-energy surface for protein folding with single-molecule fluorescence spectroscopy. *Nature.* 419:743–747.

26. Lipman, E. A., B. Schuler, O. Bakajin, and W. A. Eaton. 2003. Single-molecule measurement of protein folding kinetics. *Science.* 301:1233–1235.

27. Klostermeier, D., and D. P. Millar. 2001. RNA conformation and folding studied with fluorescence resonance energy transfer. *Methods.* 23:240–254.

28. Ishii, Y., T. Yoshida, T. Funatsu, T. Wazawa, and T. Yanagida. 1999. Fluorescence resonance energy transfer between single fluorophores attached to a coiled-coil protein in aqueous solution. *Chem. Phys.* 247:163–173.

29. Deniz, A. A., M. Dahan, J. R. Grunwell, T. J. Ha, A. E. Faulhaber, D. S. Chemla, S. Weiss, and P. G. Schultz. 1999. Single-pair fluorescence resonance energy transfer on freely diffusing molecules: observation of Förster distance dependence and subpopulations. *Proc. Natl. Acad. Sci. USA.* 96:3670–3675.

30. Burgess, R. R., and J. J. Jendrisak. 1975. A procedure for the rapid, large-scale purification of *Escherichia coli* DNA-dependent RNA polymerase involving Polymin P precipitation and DNA-cellulose chromatography. *Biochemistry.* 14:4634–4638.

31. Kim, H. D., G. U. Nienhaus, T. Ha, J. W. Orr, J. R. Williamson, and S. Chu. 2002. Mg^{2+}-dependent conformational change of RNA studied by fluorescence correlation and FRET on immobilized single molecules. *Proc. Natl. Acad. Sci. USA.* 99:4284–4289.

32. Lakowicz, J. R. 1999. Principles of Fluorescence Spectroscopy, 2nd Ed. Plenum, New York.

33. Coban, O. 2004. A fluorescence resonance energy transfer study of protein-nucleic acid complexes: RNA polymerase and Lac repressor. (PhD Thesis.). University of Ulm, Germany.

34. Groll, J., E. V. Amirgoulova, T. Ameringer, C. D. Heyes, C. Rocker, G. U. Nienhaus, and M. Moller. 2004. Biofunctionalized, ultrathin coatings of cross-linked star-shaped poly(ethylene oxide) allow reversible folding of immobilized proteins. *J. Am. Chem. Soc.* 126:4234–4239.

35. Amirgoulova, E. V., J. Groll, C. D. Heyes, T. Ameringer, C. Rocker, M. Moller, and G. U. Nienhaus. 2004. Biofunctionalized polymer surfaces exhibiting minimal interaction towards immobilized proteins. *ChemPhysChem.* 5:552–555.

36. Heyes, C. D., A. Y. Kobitski, E. V. Amirgoulova, and G. U. Nienhaus. 2004. Biocompatible surfaces for specific tethering of individual protein molecules. *J. Phys. Chem. B.* 108:13387–13394.

37. Kuzmenkina, E. V., C. D. Heyes, and G. U. Nienhaus. 2005. Single-molecule Förster resonance energy transfer study of protein dynamics under denaturing conditions. *Proc. Natl. Acad. Sci. USA.* 102:15471–15476.

38. Ying, L. M., M. I. Wallace, S. Balasubramanian, and D. Klenerman. 2000. Ratiometric analysis of single-molecule fluorescence resonance energy transfer using logical combinations of threshold criteria: a study of 12-mer DNA. *J. Phys. Chem. B.* 104:5171–5178.

39. Widengren, J., E. Schweinberger, S. Berger, and C. A. M. Seidel. 2001. Two new concepts to measure fluorescence resonance energy transfer via fluorescence correlation spectroscopy: theory and experimental realizations. *J. Phys. Chem. A.* 105:6851–6866.

40. Hagerman, P. J. 1988. Flexibility of DNA. *Annu. Rev. Biophys. Biophys. Chem.* 17:265–286.

41. Clegg, R. M., A. I. H. Murchie, A. Zechel, and D. M. J. Lilley. 1993. Observing the helical geometry of double-stranded DNA in solution by fluorescence resonance energy transfer. *Proc. Natl. Acad. Sci. USA.* 90:2994–2998.

42. Korzheva, N., A. Mustaev, M. Kozlov, A. Malhotra, V. Nikiforov, A. Goldfarb, and S. A. Darst. 2000. A structural model of transcription elongation. *Science.* 289:619–625.

43. Kuznedelov, K., N. Korzheva, A. Mustaev, and K. Severinov. 2002. Structure-based analysis of RNA polymerase function: the largest subunit's rudder contributes critically to elongation complex stability and is not involved in the maintenance of RNA-DNA hybrid length. *EMBO J.* 21:1369–1378.

44. Daube, S. S., and P. H. von Hippel. 1992. Functional transcription elongation complexes from synthetic RNA-DNA bubble duplexes. *Science.* 258:1320–1324.

45. Daube, S. S., C. R. Hart, and P. H. von Hippel. 1994. Coupling of RNA displacement and intrinsic termination in transcription from synthetic RNA-DNA bubble duplex constructs. *Proc. Natl. Acad. Sci. USA.* 91:9539–9543.

46. Daube, S. S., and P. H. von Hippel. 1994. RNA displacement pathways during transcription from synthetic RNA-DNA bubble duplexes. *Biochemistry.* 33:340–347.

47. Parkhurst, L. J., K. M. Parkhurst, R. Powell, J. Wu, and S. Williams. 2002. Time-resolved fluorescence resonance energy transfer studies of DNA bending in double-stranded oligonucleotides and in DNA-protein complexes. *Biopolymers.* 61:180–200.

48. Levin, J. R., B. Krummel, and M. J. Chamberlin. 1987. Isolation and properties of transcribing ternary complexes of *Escherichia coli* RNA polymerase positioned at a single template base. *J. Mol. Biol.* 196: 85–100.

49. Krummel, B., and M. J. Chamberlin. 1989. RNA chain initiation by *Escherichia coli* RNA polymerase. Structural transitions of the enzyme in early ternary complexes. *Biochemistry.* 28:7829–7842.

50. Holstege, F. C. P., U. Fiedler, and H. T. M. Timmers. 1997. Three transitions in the RNA polymerase II transcription complex during initiation. *EMBO J.* 16:7468–7480.

51. Wilson, K. S., C. R. Conant, and P. H. von Hippel. 1999. Determinants of the stability of transcription elongation complexes: interactions of the nascent RNA with the DNA template and the RNA polymerase. *J. Mol. Biol.* 289:1179–1194.

52. Greive, S. J., and P. H. von Hippel. 2005. Thinking quantitatively about transcriptional regulation. *Nat. Rev. Mol. Cell Biol.* 6: 221–232.